Sea-swell interaction as a mechanism for the generation of freak waves

A. Regev,[1] Y. Agnon,[1,a)] M. Stiassnie,[1] and O. Gramstad[2]
[1]*Faculty of Civil and Environmental Engineering, Technion, Haifa 32000, Israel*
[2]*Department of Mathematics, University of Oslo, P.O. Box 1053, Blindern, NO-0316 Oslo, Norway*

(Received 2 January 2008; accepted 18 September 2008; published online 18 November 2008)

The probability of freak waves in an inhomogeneous ocean is studied by integration of Alber's equation. The special phase structure of the inhomogeneous disturbance, required for instability, is provided by bound waves, generated by the quadratic interaction of the stochastic sea with a deterministic, long swell. The probability of freak waves higher than twice the significant wave height increases by a factor of up to 20 compared to the classical value given by Rayleigh's distribution. The probability of exceptionally high freak waves, with height larger than three times the significant wave height, is shown to increase some 30 000-fold compared to that given by the Rayleigh distribution, which renders their encounter feasible. © *2008 American Institute of Physics*. [DOI: 10.1063/1.3012542]

I. INTRODUCTION

Longuet–Higgins[1] showed that the wave heights in a wave field with a narrow spectrum, within the theory of linear waves, are Rayleigh distributed. From the Rayleigh distribution one can calculate that the probabilities for waves that are higher than twice or three times the significant wave height are 3×10^{-4} and 10^{-8}, respectively. The latter is such an extremely rare event that it would require an unrealistic stay in a stormy area for 30 years or so to encounter these exceptional freak waves. To encounter the former, a 10 h stay may suffice.

In recent years a few authors have used the nonlinear Schrödinger equation and its extensions, in combination with Monte Carlo simulations, to show that nonlinear interactions can increase the frequency of freak-wave occurrence by more than tenfold provided that the sea is very long crested or basically unidirectional; see Ref. 2 and the references therein. Extensive literature surveys on freak waves can be found in Refs. 3–5.

Freak waves may be an essentially inhomogeneous phenomenon. They occur at isolated places and times. Thus it is of interest to study their statistics using a model for inhomogeneous seas, namely, Alber's[6] equation. Alber's[6] equation designed for treating inhomogeneous wave fields, albeit with narrow spectra, was used by him and others to study the instability of homogeneous wave fields to inhomogeneous disturbances. Alber's[6] findings are actually the stochastic counterpart of the well-known deterministic Benjamin–Feir instability obtained for the cubic Schrödinger equation. The growth rates of the inhomogeneous instabilities are proportional to ε^2 (where ε is the wave steepness), reflecting the fact that the time scale of Alber's[6] equation is proportional to ε^{-2}. Although Abler[6] did not state it specifically, the choice of his initial small inhomogeneous disturbances discloses a certain correlation between their phases and those of the homogeneous base state.

Stiassnie *et al.*[7] found long-time recurrent evolution of Alber's[6] equation. They found that the instability which leads to subsequent recurrent evolution requires specific relations between the phases of the inhomogeneous perturbation and the primary homogeneous wave field. Here we show that such relations exist when a long, deterministic swell interacts with a short, stochastic sea.

The theoretical background is given in Sec. II, the cases studied are specified in Sec. III, and the stability diagram and the recurrent solution are presented in Sec. IV. Section V analyzes the probability density function of wave energies, and the probability of freak waves is derived and discussed in Sec. VI. The findings are assessed and discussed in Sec. VII. The calculation of the initial disturbance and some details about the numerical approach are given in Appendixes A and B.

II. THEORETICAL BACKGROUND

Alber's[6] equation for narrow-banded random surface waves on infinitely deep water written for one spatial dimension reads

$$i\left(\frac{\partial\rho}{\partial t}+\frac{1}{2}\sqrt{\frac{g}{k_0}}\frac{\partial\rho}{\partial x}\right)-\frac{1}{4}\sqrt{\frac{g}{k_0^3}}\frac{\partial^2\rho}{\partial r\,\partial x}=\sqrt{gk_0^5}\rho(x,r,t)\left[\rho\left(x+\frac{r}{2},0,t\right)-\rho\left(x-\frac{r}{2},0,t\right)\right]. \quad (1)$$

The definition of the two-point spatial correlation $\rho(x,r,t)$ is

$$\rho(x,r,t)=\left\langle A\left(x+\frac{r}{2},t\right)A^*\left(x-\frac{r}{2},t\right)\right\rangle, \quad (2)$$

where the angular brackets $\langle\ \rangle$ stand for the ensemble average. $A(x,t)$ is the complex envelope of the narrow-banded sea, related to the random free-surface elevation $\eta(x,t)$ by

a)Author to whom correspondence should be addressed. Telephone: +972-4-8292489. FAX: +972-4-8228898. Electronic mail: agnon@tx.technion.ac.il.

TABLE I. Different input parameters for seven case studies.

Case			A_1	A_2	B	C	D	E	F
Swell conditions	T_l (s)	Period	18	18	18	18	18	18	18
	a_l (m)	Amplitude	1	2	1	1	1	1	1
	λ_l (m)	Length	505	505	505	505	505	505	505
	K (m^{-1})	Wave number	0.0124	0.0124	0.0124	0.0124	0.0124	0.0124	0.0124
Initial sea conditions	T_s (s)	Peak period	10	10	10	10	10	8	12
	a_s (m)	Amplitude	4	4	4	4	4	4	4
	H_s (m)	Significant height	11.3	11.3	11.3	11.3	11.3	11.3	11.3
	λ_s (m)	Length	156	156	156	156	156	100	225
	k_0 (m^{-1})	Wave number	0.04	0.04	0.04	0.04	0.04	0.063	0.028
	W (m^{-1})	Spectral width	0.0032	0.0032	0.0065	0.0097	0.013	0.0158	0.0031
	s_0 (m^3)	Eq. (17)	1234	1234	617	411	309	253	1280
Nondimensional parameters	ε	Wave steepness	0.16	0.16	0.16	0.16	0.16	0.25	0.11
	$\tilde{W}$	Eq. (18)	0.5	0.5	1	1.5	2	1	1
	BFI	Benjamin–Feir index	1.4	1.4	0.7	0.47	0.35	0.7	0.7
	$\tilde{K}$	Eq. (18)	1.9	1.9	1.9	1.9	1.9	0.8	4
	$\tilde{\Omega}_I$	Growth rate	0.46	0.46	0.41	0.3	0.14	0.22	0
	δ	Eq. (15)	0.08	0.16	0.08	0.08	0.08	0.126	0.056

$$2\eta(x,t) = A(x,t)e^{i(k_0x-\sqrt{gk_0}t)} + * . \tag{3}$$

The correlation for a homogeneous ocean at $r=0$ is given by the integral of the energy spectrum

$$\rho_h(r=0) = \int_{-\infty}^{\infty} S(k)dk \tag{4}$$

and, thus,

$$\rho_h(r=0) \propto H_{\mathrm{rms0}}^2, \tag{5}$$

where H_{rms0} is the root mean square wave height of the homogeneous ocean. In a similar way, based on Eq. (3.2) of Ref. 7 one can assume that for an inhomogeneous ocean,

$$\rho(x,r=0,t) \propto H_{\mathrm{rms}}^2, \tag{6}$$

where H_{rms}^2 is a measure of the average energy density at the point (x,t).

From Eqs. (5) and (6) one has

$$\frac{H_{\mathrm{rms0}}^2}{H_{\mathrm{rms}}^2} = \frac{\rho_h(r=0)}{\rho(x,r=0,t)}. \tag{7}$$

The Rayleigh distribution

$$P(H \geq \hat{H}) = e^{-(\hat{H}/H_{\mathrm{rms}})^2} \tag{8}$$

can be rewritten as

$$P(H/H_{\mathrm{rms0}} \geq \hat{H}/H_{\mathrm{rms0}}) = e^{-[(\hat{H}/H_{\mathrm{rms0}})(H_{\mathrm{rms0}}/H_{\mathrm{rms}})]^2}. \tag{8'}$$

Substituting Eq. (7) into Eq. (8′) gives that for a chosen value of ρ,

$$P(H/H_{\mathrm{rms0}} > \hat{H}/H_{\mathrm{rms0}}) = \exp\left\{-\left(\frac{\hat{H}}{H_{\mathrm{rms0}}}\right)^2 \frac{\rho_h}{\rho}\right\}. \tag{8''}$$

However, the probability to obtain values of ρ in the range $(\rho, \rho+\delta\rho)$ is given by pdf(ρ), which stands for the probability density function of $\rho(x,r=0,t)$. Thus, the probability to obtain $H>\hat{H}$ throughout the spatial and temporal evolutions of ρ is given by

$$P(H/H_{\mathrm{rms0}} \geq \hat{H}/H_{\mathrm{rms0}}) = \int \mathrm{pdf}(\rho) e^{-(\hat{H}/H_{\mathrm{rms0}})^2(\rho_h/\rho)} d\rho. \tag{9}$$

The probability density function of $\rho(x,0,t)$ is discussed and calculated in Sec. V.

III. SEVEN CASE STUDIES

In the present article seven different oceanic combinations of sea and swell conditions are considered. The initial condition of the sea is assumed to have a Gaussian spectrum, and the swell is assumed to be monochromatic.

The period of the long swell is $T_l=18$ s for all seven cases (which corresponds to the wavelength $\lambda_s=505$ m), and the amplitude of the swell, a_l, is taken to be 1 or 2 m.

The peak period of the shorter sea is denoted by T_s and varies from 8 to 10 and to 12 s. The initial Gaussian spectra of the sea are given by

$$S(k) = 1.45 s_o e^{-1.64[(k-k_0)/W]^2}, \tag{10}$$

where k_0 is the peak wave number of the sea, $2W$ is the spectral width, and $2s_0$ W is the total energy density. The values of k_0, W, s_0, and a few other characteristic quantities are given in Table I. Note that all seven initial seas have the same significant wave height $H_s=11.3$ m.

IV. STABILITY DIAGRAM AND RECURRENT SOLUTIONS

The evolution of the solution of Eq. (1) has been calculated numerically in Ref. 7 using the following nondimensional variables

$$\tilde{\rho} = \frac{k_0^2}{\varepsilon^2}\rho, \quad \tilde{\xi} = \varepsilon k_0\left(x - \frac{1}{2}\sqrt{\frac{g}{k_0}}t\right),$$

$$\tilde{\tau} = (\varepsilon^2\sqrt{gk_0})t, \quad \tilde{r} = \varepsilon k_0 r,$$

where ε is the steepness of the sea.

In these variables Eq. (1) reduces to

$$i\frac{\partial\tilde{\rho}}{\partial\tilde{\tau}} - \frac{1}{4}\frac{\partial^2\tilde{\rho}}{\partial\tilde{\xi}\,\partial\tilde{r}} - \tilde{\rho}[\tilde{\rho}(\tilde{\xi}+\tilde{r}/2,0) - \tilde{\rho}(\tilde{\xi}-\tilde{r}/2,0)] = 0. \quad (11)$$

The values of $\tilde{\rho}(\tilde{\xi},\tilde{r},\tilde{\tau})$ are calculated for different initial conditions, defined as

$$\rho(x,r,t=0) = \rho_h(r) + \delta\rho_1(x,r,t=0), \quad (12)$$

where

$$\rho_h(r) = \int_{-\infty}^{\infty} e^{i(k-k_0)r}S(k)dk \quad (13)$$

and

$$\rho_1(x,r,t) = R(r)\cos(Kx). \quad (14)$$

For a sea-swell interaction (see details in Appendix A), Eq. (A7) reads

$$R(r) = \rho_h\left(\frac{K}{k_0}\cos(Kr/2) + i\,\sin(Kr/2)\right) \quad \text{and} \quad \delta = 2a_l k_0. \quad (15)$$

K and k_0 are the swell and sea wave numbers, respectively, and the initial homogeneous correlation is

$$\tilde{\rho}_h(\tilde{r}) = \frac{1.133\sqrt{\pi}}{4}e^{-[(\tilde{r}\tilde{W})^2/6.45]}. \quad (16)$$

The governing nondimensional parameters as defined in Ref. 7 are

$$\varepsilon = a_s k_0 = \sqrt{4s_0 W k_0} = o(1), \quad (17)$$

$$\tilde{\Omega}_I = \Omega_I/\varepsilon^2\sqrt{gk_0}, \quad \tilde{K} = K/\varepsilon k_0, \quad \text{and} \quad \tilde{W} = W/\varepsilon k_0, \quad (18)$$

where $\tilde{\Omega}_I$ is the nondimensional growth rate.

All seven cases of Table I are marked on the stability diagram given in Fig. 1.

Cases E, B, and F are all for $\tilde{W}=1$ but for different $\tilde{K}$. Case F falls in the stable zone and no freak waves, which result from the swell-sea interaction, are expected for this case. Cases E and B are in the unstable zone, where freak-waves will emerge from the evolution. However, Stiassnie *et al.*[7] found that unstable cases outside the shaded zone will produce simple recurrence, whereas those in the shaded zone produce complex recurrence. The statistical treatment of cases within the shaded zone is more complicated and is not considered in this paper.

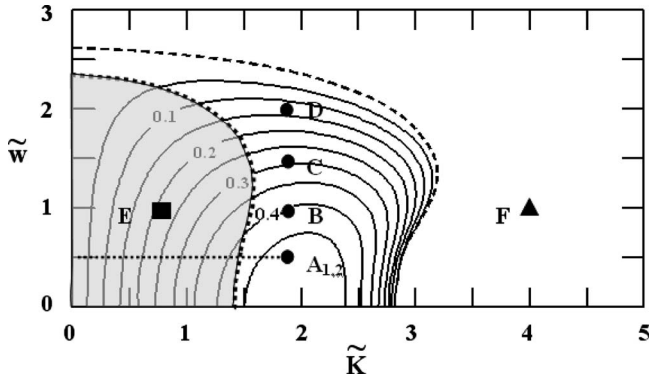

FIG. 1. Stability diagram: Isolines of the nondimensional growth rate $\tilde{\Omega}_I$ for a Gaussian spectrum. T_s=8 s (triangle), T_s=10 s (circles), and T_s=12 s (square).

Cases A_1, B, C, and D of Table I and Fig. 1 have been chosen in order to assess the influence of the spectral width on the probability of freak waves. These four cases have all the same $\tilde{K}$ and δ. A comparison between cases A_1 and A_2 will enable us to assess the influence of δ, i.e., of the amplitude of the swell, see Eq. (15). One should note the simple relation between our $\tilde{W}$ and the Benjamin–Feir index (BFI) of Janssen:[8] $\text{BFI} = 1/\sqrt{2}\tilde{W}$.

The numerical results for the values of $\tilde{\rho}_m(\tilde{\tau})$, i.e., of the maximum value of $\tilde{\rho}(\tilde{\xi},0,\tilde{\tau})$, taken for a chosen $\tilde{\tau}$ and for all possible $\tilde{\xi}$, are shown in Fig. 2. Note that only one typical cycle of the recurring evolution is drawn. The numerical approach is outlined in Appendix B.

Comparing case A_2 to case A_1, one can see that as the swell amplitude becomes larger, the recurrence period shortens but the maximum value of $\tilde{\rho}$ remains similar. One can also see that as the initial spectral width becomes smaller (that is, larger growth rate and larger BFI) the maximum values of $\tilde{\rho}$ get larger and the recurrence period shortens. The nondimensional periods of the cycles drawn in Fig. 2 are 14, 17.5, 19.5, 26, and 52 for A_2, A_1, B, C, and D, respectively.

V. THE PROBABILITY DENSITY FUNCTION OF $\tilde{\rho}(\tilde{\xi},0,\tilde{\tau})$

In order to find pdf$(\tilde{\rho})$ the following steps were taken: First, 100 locations evenly distributed along the $\tilde{\xi}$ axis from 0

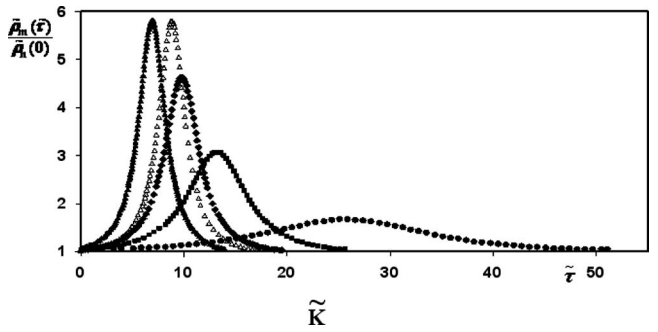

FIG. 2. A typical cycle of the long-time recurring evolution of $\tilde{\rho}_m(\tilde{\tau})/\tilde{\rho}_h(0)$ for A_2 (▲), A_1 (△), B (♦), C (■), and D (●).

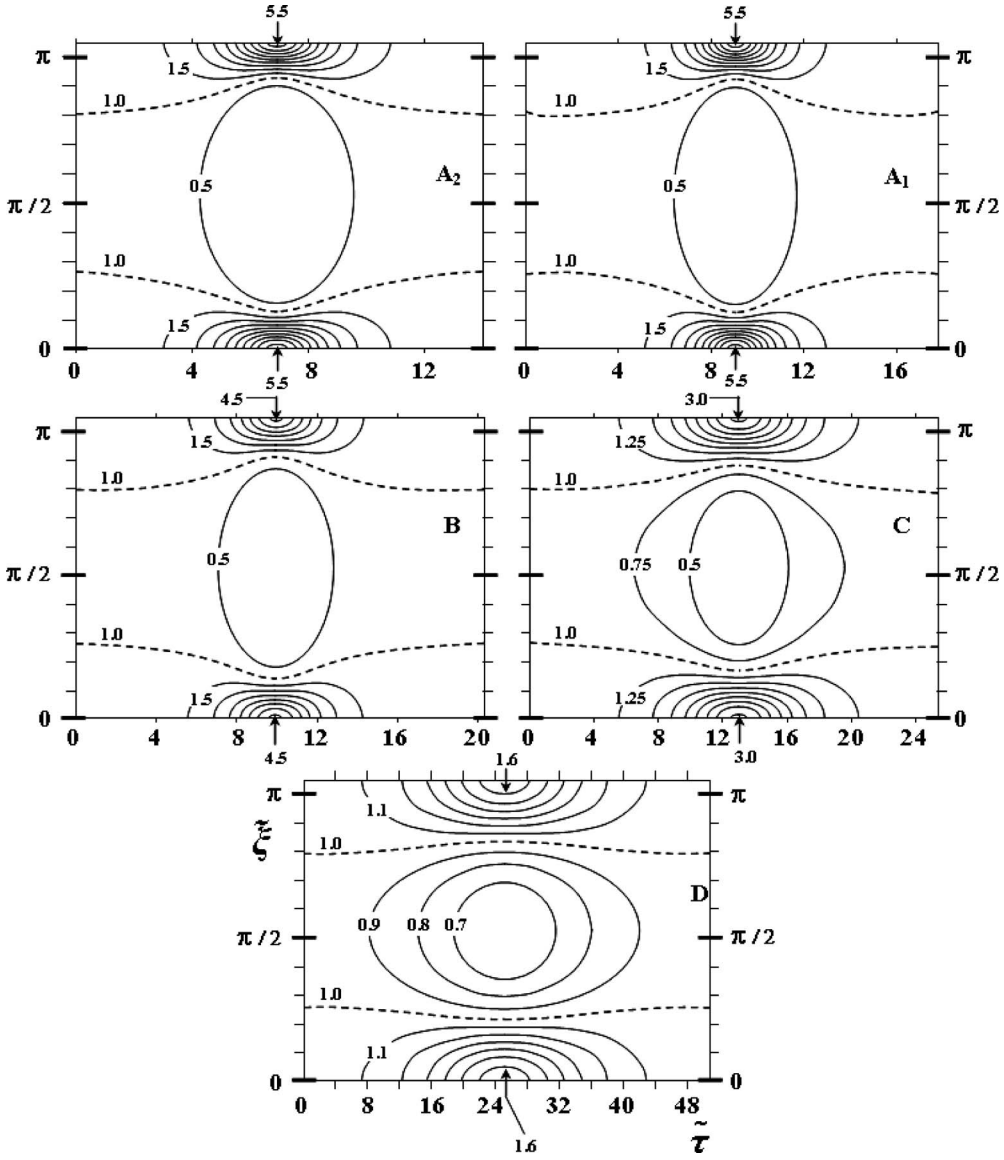

FIG. 3. Isolines of $\tilde{\rho}(\tilde{\xi},0,\tilde{\tau})/\tilde{\rho}_h(0)$.

to $2\pi/\tilde{K}$ were taken. During one recurrence cycle, $\tilde{\rho}$ was sampled at 100 evenly distributed sampling times, so that 10^4 $\tilde{\rho}(\tilde{\xi},0,\tilde{\tau})$ values were used to establish pdf$(\tilde{\rho})$. The isolines of $\tilde{\rho}/\tilde{\rho}_h$ are plotted in Fig. 3 for the above mentioned five different cases. In these plots the values were shifted on the $\tilde{\xi}$ axis so that the maximum values are at $\tilde{\xi}=0$ and $\tilde{\xi}=2\pi/\tilde{K}$. The curves were also slightly smoothed.

Second, the 10 000 values were arranged from the lowest to the highest and divided into 100 evenly spaced increments in $\tilde{\rho}$. The probability of each increment was calculated as the number of elements within the increment divided by 10 000. Figure 4 presents the probability density function of $\tilde{\rho}/\tilde{\rho}_h$ by a bar diagram (to ease comparison, the widths of the bins in all bar diagrams are equal) and the probability function (the probability to obtain a value smaller or equal to $\tilde{\rho}/\tilde{\rho}_h$) by the solid line for the five different cases. From Figs. 3 and 4 one can see that for cases A_1 and A_2 many bins are activated and that the number of active bins reduces when the spectral width grows.

VI. THE PROBABILITY OF FREAK WAVES

The probability function of the wave height, Eq. (9), is calculated on the basis of the known values of pdf$(\tilde{\rho})$ shown in Fig. 4.

The values of the wave-height probabilities for an inhomogeneous ocean are compared with those of the homogeneous case given by Eq. (8). In Fig. 5 one can see the freak-wave probability values, i.e., the probability for waves with $\hat{H}\geq 2.85H_{\mathrm{rms0}}\approx 2H_s$. The inset shows the probability function for the Rayleigh distribution, which corresponds to a homogeneous sea, and the probability obtained from the calculation made using Alber's[6] equation for case A_2. As one can see from Fig. 5 the probability up to $\hat{H}\geq 1.4H_{\mathrm{rms0}}$ is greater for the Rayleigh distribution, but after the intersection point the probability is greater for the results obtained from Alber's[6] equation, the intersection values for cases A_1, B, C, and D are in the range $\hat{H}/H_{\mathrm{rms0}}\in(1.4,1.7)$.

From the results given by Fig. 5 one can draw the following conclusions:

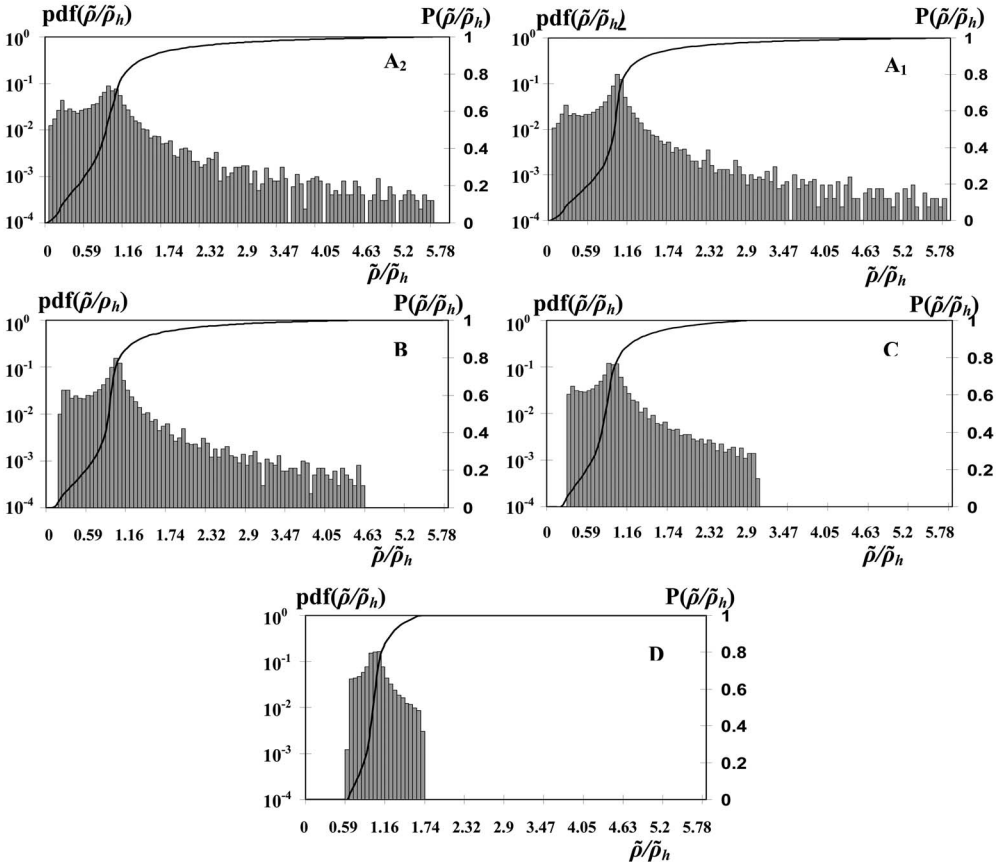

FIG. 4. Probability density function pdf($\tilde{\rho}/\tilde{\rho}_h$) and probability function $P(\tilde{\rho}/\tilde{\rho}_h)$ as functions of $\tilde{\rho}/\tilde{\rho}_h$.

- There is a strong effect of the spectral width W, which together with the sea wave number and the sea amplitude sets the growth rate, and can also be related to the BFI. Case A_1 gives 50/10 000 waves higher than $2.85H_{\mathrm{rms0}}(=2H_s)$, as opposed to case D in which only 6/10 000 are higher than $2.85H_{\mathrm{rms0}}$, which is closer to the Rayleigh distribution (for which 3/10 000 waves are higher than $2H_s$).
- There is a weaker effect of the swell amplitude a_l, which affects the size of the small inhomogeneous disturbance δ [see Eq. (15)]. In case A_2, δ is double the value of δ in case A_1 (0.16 compared to 0.08). In case A_2 60/10 000 waves are higher than $2.85H_{\mathrm{rms0}}$, compared to 50/10 000 in case A_1.
- The probability of exceptionally high freak waves, with wave heights higher than three times that of the significant wave height, increases from the "almost never" value of 10^{-8} for the Rayleigh distribution to 2/10 000 for case B, 3/10 000 for case A1, and 4/10 000 for case A_2. These values make the encounter of exceptionally high freak waves more likely.

Note that for non-narrow-banded spectra, albeit within the linear theory approximation, Tayfun[9] found that the prob-

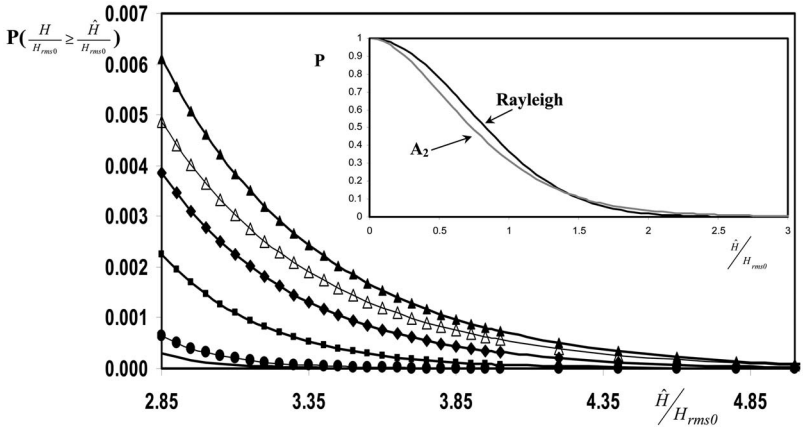

FIG. 5. The probability of freak waves ($\hat{H}/H_{\mathrm{rms0}} \geq 2.85$) for the Rayleigh distribution (—) and the probability obtained from Alber's equation (Ref. 6): case A_2 (▲), case A_1 (△), case B (◆), case C (■), and case D (●). The inset shows the probability function for the Rayleigh distribution (black line) and case A_2 (gray line).

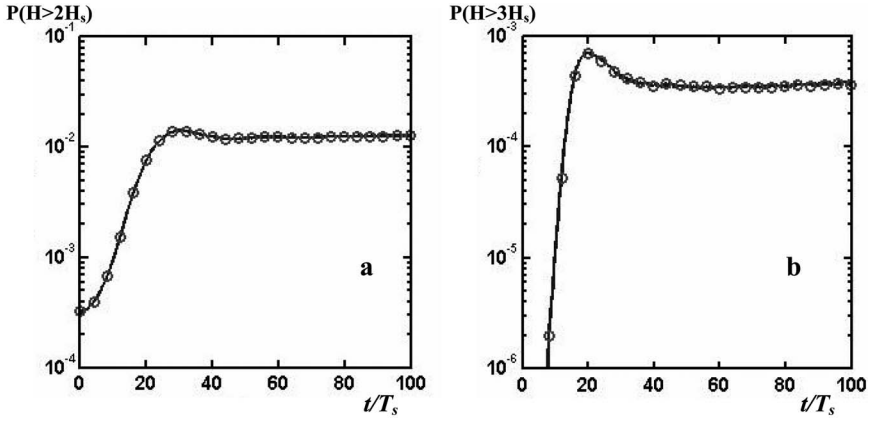

FIG. 6. Probability of freak waves as a function of time from Monte Carlo simulations with the nonlinear Schrödinger equation for (a) $H \geq 2H_s$ and (b) exceptionally freak waves $H \geq 3H_s$.

ability for the very high waves is overpredicted by the Rayleigh distribution.

VII. DIRECT SIMULATION AND SUMMARY

In order to confirm the results for the probability of freak waves, described in Sec. VI, we carried out "Monte Carlo" simulations with solutions of the nonlinear Schrödinger equations; for A_s, the complex wave envelopes of the sea [A is defined in Eq. (3)]:

$$i\left(\frac{\partial A_s}{\partial t}+\frac{1}{2}\sqrt{\frac{g}{k_0}}\frac{\partial A_s}{\partial x}\right)-\frac{g^{1/2}}{8k_0^{3/2}}\frac{\partial^2 A_s}{\partial x^2}=\frac{g^{1/2}k_0^{5/2}}{2}|A_s|^2A_s. \tag{19}$$

The numerical solution of Eq. (19) was carried out using the split-step Fourier method used by Shemer *et al.*[10] and by Lo and Mei.[11] The computation domain consisted of $512\lambda_s$, and an average over 2000 realizations was taken.

Case A_2 of Table I was chosen for comparison. The probability of freak waves, as well as the probability for exceptionally high freak waves, as a function of time is presented in Fig. 6. The asymptotic probabilities for large times of $H \geq 2H_s$ and $H \geq 3H_s$ from Fig. 6 are 120/10 000 and 4/10 000, compared to 60/10 000 and 5/10 000, which were obtained from Alber's[6] equation, respectively. We consider this to be a fair agreement in view of the difference described below.

The initial sea that we have substituted into Alber's[6] equation is strictly homogeneous, and an additional inhomogeneous disturbance is required in order to obtain nontrivial solutions. One could think about different physical mechanisms that can induce the required inhomogeneity.

In the solution that used Alber's[6] equation, the activating inhomogeneous disturbances are provided by bound waves, which are generated through quadratic interaction of the stochastic sea with a deterministic *swell*, as explained in Appendix A. This is just one possible source of inhomogeneity. An alternative source is the inevitably limited number of realizations in a Monte Carlo simulation.

Thus, it is not necessary to have long waves for the inhomogeneity to arise. Indeed, the swell, as such, is not involved in the 2000 solutions of the nonlinear Schrödinger equation (19), which were used for the Monte Carlo simulation. However, using the 2000 random sets of initial condition, one can calculate the two-point spatial correlation $\rho(x,r,t)$ at $t=0$, see Fig. 7. From Fig. 7, it is quite clear that the ensemble of 2000 realizations fails to produce a homogeneous sea, for which ρ must be independent of x. The matter of fact is that a closer observation of the fine structure of the lines $|\rho(x,r,0)|=\text{const}$ reveals length scales in x of the order of about $10\lambda_s$, which correspond to $\tilde{K}\approx 0.6$. On the stability diagram, see Fig. 1, these length scales would be located on the horizontal line $\tilde{w}=0.5$ (dashed line in the figure), well within the shaded *complex recurrence zone*.

Thus, it seems that the difference in the nature of the initial inhomogeneous disturbances is the main reason for the somewhat different results of both models.

To summarize we have the following:

- Alber's[6] equation was used to study the statistics of freak waves in a unidirectional inhomogeneous sea. The inhomogeneity arises due to the interaction of a deterministic, long swell with a stochastic, short sea.

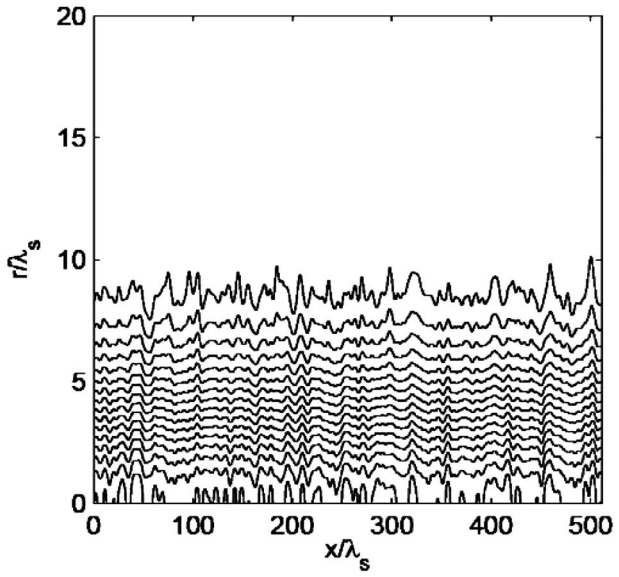

FIG. 7. Isolines of the modulus of the two-point spatial correlation of the sea at $t=0$ and for case A_2. The ensemble average was taken over 2000 realizations

- The probability of freak waves increased up to 20 times (compared to the reference, Rayleigh distribution) as the spectral width of the sea decreases and the amplitude of the swell increases. The probability for exceptionally high freak waves was increased by a factor of about 30 000.
- The results were compared to those obtained by Monte Carlo simulations with the nonlinear Schrödinger equations.
- The more general and more common case, where the wind-wave system and the swell propagate in different directions, requires a much heavier numerical effort and is left for a future study.

ACKNOWLEDGMENTS

This research was supported by the Israel Science Foundation (Grant No. 695/04) and by the U.S.–Israel Binational Science Foundation (Grant No. 2004-205).

APPENDIX A: THE INITIAL DISTURBANCE

Using the notation of Secs. 14.2 and 14.3 in Ref. 12 and assuming the coexistence of a swell with a single mode $\tilde{B}_0^l$ and a sea which consists of many modes $\tilde{B}_n^s$:

$$\varepsilon\tilde{B}(k,t)=\sum_n \tilde{B}_n^s\delta(k-k_n^s)+\tilde{B}_0^l\delta(k-k^l); \tag{A1}$$

One can use their Eqs. (14.3.1), (14.3.3), and (14.2.15) to obtain the following expression for the free-surface elevation:

$$\eta(x,t)=\frac{1}{2\pi}\sqrt{\frac{\omega(k^l)}{2g}}\{\tilde{B}_0^l e^{i[k^l x-\omega(k^l)t]}+\text{c.c}\}+\frac{1}{2\pi}\sum_n\left\{\sqrt{\frac{\omega(k_n^s)}{2g}}\tilde{B}_n^s e^{i[k_n^s x-\omega(k_n^s)t]}\right.$$
$$+\frac{1}{4\pi}\left[\frac{\omega(k_n^s+k^l)}{[\omega(k^l)\omega(k_n^s)]^{1/2}}\left[\frac{\omega(k^l)\omega(k_n^s)}{g}\right]^2\frac{\omega(k_n^s+k^l)}{\omega(k^l)\omega(k_n^s)}\tilde{B}_n^s\tilde{B}_0^l e^{i\{(k_n^s+k^l)x-[\omega(k_n^s)+\omega(k^l)]t\}}\right.$$
$$\left.\left.-\left[\frac{\omega(k_n^s)}{\omega(k^l)}\right]^{1/2}\left[\frac{\omega(k_n^s-k^l)\omega(k^l)}{g}\right]^2\frac{1}{\omega(k^l)}e^{i\{(k_n^s-k^l)x-[\omega(k_n^s)-\omega(k^l)]t\}}\tilde{B}_n^s(\tilde{B}_0^l)^*+\text{c.c}\right]\right\}. \tag{A2}$$

The above expression includes the free modes of the swell and the sea, as well as the bound modes of their mutual interaction.

Substituting Eq. (A2) into Eqs. (2) and (3), in Sec. II, and assuming that the sea modes $\tilde{B}_n^s$ have random phases leads to

$$\rho(x,r,0)=\sum_n\frac{\omega(k_n^s)}{2g\pi^2}|\tilde{B}_n^s|^2e^{i(k_n^s-k^s)r}\left[1+\frac{1}{2\pi}\left(\frac{\omega(k^l)}{2g}\right)^{1/2}(k_n^s+k^l)\tilde{B}_0^l e^{ik^l(x+r/2)}-\frac{1}{2\pi}\left(\frac{\omega(k^l)}{2g}\right)^{1/2}(k_n^s-k^l)(\tilde{B}_0^l)^*e^{-ik^l(x+r/2)}\right.$$
$$\left.+\frac{1}{2\pi}\left(\frac{\omega(k^l)}{2g}\right)^{1/2}(k_n^s+k^l)(\tilde{B}_0^l)^*e^{-ik^l(x-r/2)}-\frac{1}{2\pi}\left(\frac{\omega(k^l)}{2g}\right)^{1/2}(k_n^s-k^l)\tilde{B}_0^l e^{ik^l(x-r/2)}\right]. \tag{A3}$$

From Eq. (14.5.5) in Ref. 12,

$$a_n=\frac{1}{\pi}|B_n|\left(\frac{\omega_n}{2g}\right)^{1/2},\quad a_l=\frac{1}{\pi}|B_l|\left(\frac{\omega_l}{2g}\right)^{1/2}, \tag{A4}$$

and substituting Eq. (A4) and $B_0^l=|B_0^l|e^{i\theta_l}$ into Eq. (A3) gives

$$\rho(x,r,0)=\sum_n\frac{a_n^2}{2}e^{i(k_n^s-k^s)r}\left\{1+\frac{a_l}{2}[e^{i\theta_l}(k_n^s e^{ik^l(x+r/2)}+k^l e^{ik^l(x+r/2)}\right.$$
$$-k_n^s e^{ik^l(x-r/2)}+k^l e^{ik^l(x-r/2)})+e^{-i\theta_l}(k_n^s e^{-ik^l(x-r/2)}$$
$$\left.+k^l e^{-ik^l(x-r/2)}-k_n^s e^{-ik^l(x+r/2)}+k^l e^{-ik^l(x+r/2)})]\right\}. \tag{A5}$$

Using Eq. (4) and recalling the narrowness of the sea spectrum, which justifies replacing k_n^s by k^s in the curly brackets of Eq. (A5), gives

$$\rho(x,r,0)=\rho_h\left[1+2a_l k^s\cos(k^l x+\theta_l)\left(\frac{k^l}{k^s}\cos(k^l r/2)+i\sin(k^l r/2)\right)\right]. \tag{A6}$$

Comparing Eq. (A6) with Eqs. (12) and (14) and recognizing that $k^l=K$, $k^s=k_0$ results in

$$R(r)=\rho_h\left(\frac{K}{k_0}\cos(Kr/2)+i\sin(Kr/2)\right),$$
$$\delta=2a_l k_0=2\varepsilon_l\frac{k_0}{K}. \tag{A7}$$

Equation (A7) is the final result of this appendix and it is identical to Eq. (15), in Sec. IV, of this paper.

APPENDIX B: THE NUMERICAL APPROACH

Equation (11) was formulated as a finite difference scheme, approximating the time derivative by a forward difference and the $\tilde{\xi}$ and $\tilde{r}$ derivatives by central differences:

$$i\left[\frac{\tilde{\rho}_{(n,j,\ell+1)}-\tilde{\rho}_{(n,j,\ell)}}{\Delta\tilde{\tau}}\right]-\frac{1}{16\Delta\tilde{\xi}\Delta\tilde{r}}\{\tilde{\rho}_{(n+1,j+1,\ell)}-\tilde{\rho}_{(n-1,j+1,\ell)}-[\tilde{\rho}_{(n+1,j-1,\ell)}-\tilde{\rho}_{(n-1,j-1,\ell)}]\}-\tilde{\rho}_{(n,j,\ell)}\{\tilde{\rho}_{[n+j\Delta\tilde{r}/(2\Delta\tilde{\xi}),0,\ell]}-\tilde{\rho}_{[n-j\Delta\tilde{r}/(2\Delta\tilde{\xi}),0,\ell]}\}=0, \quad \text{(B1)}$$

where the index n represents points along the $\tilde{\xi}$ axis, $\tilde{\xi}=n\Delta\tilde{\xi}$, $n=0,1,2,\ldots,N$, and $N+1$ is the number of points along this axis. The subscript j represents points along the $\tilde{r}$ axis, where $\tilde{r}=j\Delta\tilde{r}$, $j=0,1,2,\ldots,M$, and $M+1$ is the number of points along the $\tilde{r}$ axis. ℓ represents time steps where $\tilde{\tau}=\ell\Delta\tilde{\tau}$, $\ell=0,1,2,\ldots$.

The numerical time stepping scheme is formulated as follows:

$$\tilde{\rho}_{(n,j,\ell+1)}=\tilde{\rho}_{(n,j,\ell)}-\frac{i\Delta\tilde{\tau}}{16\Delta\tilde{\xi}\Delta\tilde{r}}\{\tilde{\rho}_{(n+1,j+1,\ell)}-\tilde{\rho}_{(n-1,j+1,\ell)}-[\tilde{\rho}_{(n+1,j-1,\ell)}-\tilde{\rho}_{(n-1,j-1,\ell)}]\}-i\Delta\tilde{\tau}\tilde{\rho}_{(n,j,\ell)}\times\{\tilde{\rho}_{[n+j\Delta\tilde{r}/(2\Delta\tilde{\xi}),0,\ell]}-\tilde{\rho}_{[n-j\Delta\tilde{r}/(2\Delta\tilde{\xi}),0,\ell]}\}. \quad \text{(B2)}$$

We restrict ourselves to periodic solutions in $\tilde{\xi}$ so that on the boundary $\tilde{\xi}=\tilde{\xi}_{\text{end}}$, $\tilde{\rho}_{(N,j,\ell)}=\tilde{\rho}_{(0,j,\ell)}$.

The last term on the right-hand side of Eq. (B2) depends on values of $\tilde{\rho}$ at $\tilde{\xi}=n\Delta\tilde{\xi}+j\Delta\tilde{r}/2$ which can be larger than $\tilde{\xi}_{\text{end}}=N\Delta\tilde{\xi}$. Again, the periodicity condition is used: $\tilde{\rho}(\tilde{\xi}+2p\pi,\tilde{r},\tilde{\tau})=\tilde{\rho}(\tilde{\xi},\tilde{r},\tilde{\tau})$, where $p=1,2,\ldots$, or $\tilde{\rho}_{(n+pN,j,\ell)}=\tilde{\rho}_{(n,j,\ell)}$.

The values of $\tilde{\rho}$ along $\tilde{r}=0$ depend on points outside the domain $0\le\tilde{r}\le\tilde{r}_{\text{end}}$. Specifically, the second term on the right-hand side of Eq. (B2) depends on $\tilde{\rho}_{(n,-1,\ell)}$. From the definition of $\tilde{\rho}$, Eq. (2), we see that $\tilde{\rho}(\tilde{\xi},-\tilde{r},\tilde{\tau})=\tilde{\rho}^{*}(\tilde{\xi},\tilde{r},\tilde{\tau})$, so one can calculate the value of $\tilde{\rho}$ along $\tilde{r}=0$ from the condition $\tilde{\rho}_{(n,-1,\ell)}=\tilde{\rho}^{*}_{(n,1,l)}$.

Theoretically, the $\tilde{r}$ axis extends to infinity: however, for practical reasons, the axis must be truncated. The boundary condition that was used for large $\tilde{r}$ is given by

$$\tilde{\rho}(\tilde{\xi},\tilde{r},\tilde{\tau})=\sqrt{\tilde{\rho}(\tilde{\xi}+\tilde{r}/2,0,\tilde{\tau})\tilde{\rho}(\tilde{\xi}-\tilde{r}/2,0,\tilde{\tau})}\frac{\sin(\tilde{w}\tilde{r})}{\tilde{w}\tilde{r}}. \quad \text{(B3)}$$

For more details see Sec. 4.3 in Ref. 7.

[1] M. S. Longuet-Higgins, "On the statistical distribution of the heights of sea waves," J. Mar. Res. **11**, 1245 (1952).
[2] O. Gramstad and K. Trulsen, "Influence of crest and group length on the occurrence of freak-waves," J. Fluid Mech. **582**, 463 (2007).
[3] C. Kharif and E. Pelinovsky, "Physical mechanism of the rogue wave phenomenon," Eur. J. Mech. B/Fluids **22**, 603 (2003).
[4] M. Onorato, A. R. Osborne, M. Serio, L. Cavaleri, C. Brandini, and C. T. Stansberg, "Observation of strongly non-Gaussian statistics for random sea surface gravity waves in wave flume experiments," Phys. Rev. E **70**, 067302 (2004).
[5] N. Mori, M. Onorato, P. A. Janssen, A. R. Osborne, and M. Serio, "On the extreme statistics of long-crested deep water waves: Theory and experiments," J. Geophys. Res. **112**, C09011, DOI: 10.1029/2006JC004024 (2007).
[6] I. E. Alber, "The effects of randomness on the stability of two-dimensional surface wavetrains," Proc. R. Soc. London, Ser. A **363**, 525 (1978).
[7] M. Stiassnie, A. Regev, and Y. Agnon, "Recurrent solutions of Alber's equation for random water-wave fields," J. Fluid Mech. **598**, 245 (2008).
[8] P. A. E. M. Janssen, "Nonlinear four-wave interactions and freak-waves," J. Phys. Oceanogr. **33**, 863 (2003).
[9] M. A. Tayfun, "Distribution of crest-to-trough wave height," J. Waterway, Port, Coastal, Ocean Eng. **107**, 149 (1981).
[10] L. Shemer, E. Kit, and H.-Y. Jiao, "An experimental and numerical study of the spatial evolution of unidirectional nonlinear water-wave groups," Phys. Fluids **14**, 3380 (2002).
[11] E. Lo and C. C. Mei, "A numerical study of water-wave modulation based on a higher-order nonlinear Schrödinger equation," J. Fluid Mech. **150**, 395 (1985).
[12] C. C. Mei, M. Stiassnie, and D. K.-P. Yue, *Theory and Applications of Ocean Surface Waves*, Advanced Series on Ocean Engineering Vol. 23 (World Scientific, Singapore, 2005).